Published in final edited form as:
*Nanoscale*. 2013 November 21; 5(22): . doi:10.1039/c3nr02608f.

# Electron beam induced local crystallization of $HfO_2$ nanopores for biosensing applications

**Jiwook Shim**[1,2,3,#], **Jose Rivera**[1,3,#], and **Rashid Bashir**[1,2,3,*]

[1]Department of Bioengineering, University of Illinois at Urbana – Champaign, Urbana, IL 61801

[2]Electrical and Computer Engineering, University of Illinois at Urbana – Champaign, Urbana, IL 61801

[3]Micro and Nanotechnology Laboratory, University of Illinois at Urbana – Champaign, Urbana, IL 61801

## Abstract

We report the development of single, locally crystallized nanopores in $HfO_2$ membranes for biosensing applications. $HfO_2$ is chosen for its isoelectric point of 7.0, mechanical and chemical stability in solution, and for its potential as a high-k material for nanopore ionic field effect transistor applications. The $HfO_2$ membrane is deposited on a graphene layer suspended over a 300 nm FIB hole, where graphene is used as the mechanical support. Exposure of the membrane to a focused electron beam causes crystallization in the vicinity of the nanopore during pore formation. We investigate the effects of crystallization on the electrical and surface properties of $HfO_2$ films. Our surface analysis of $HfO_2$ reveals improved hydrophilicity of crystallized $HfO_2$, a notable advantage over the hydrophobicity of as-deposited $HfO_2$. We also demonstrate detection of dsDNA translocation through $HfO_2$ nanopores under various applied bias levels. In addition, our device architecture also presents a promising first step toward the realization of high-k $HfO_2$ nanopore transistors.

## INTRODUCTION

Nanopores continue to hold considerable promise as both a bio-sensing and as a DNA sequencing technology (see reviews[1–5]). The high sensitivity of solid-state nanopores has allowed for the successful detection of biomolecule complexes including RNA/Antibiotic complexes[6], RecA-coated double-stranded DNA[7], and methylated DNA bound to methyl-*CpG*-binding domain proteins[8]. A recent report has also demonstrated electronic discrimination of similar genes by measuring the relative distance between γPNA probes hybridized to DNA with solid-state nanopores[9]. The interdisciplinary effort from researchers to establish solid-state nanopores as a viable sequencing platform is thriving on multiple fronts including the differentiation of short single-stranded DNA[10], surface charge engineering for DNA capture[11], conductance modulation[12, 13] in nanopores, nanowire-nanopore transistors for localized detection[14], and ultra-thin membrane fabrication using graphene[15, 16].

Recently, an alternative nanopore structure has evolved from the integration of graphene with solid-state membranes for both biosensing and DNA sequencing applications[17, 18]. This

*Corresponding Author: rbashir@illinois.edu, Rashid Bashir, PhD, Abel Bliss Professor, Department of Bioengineering, Department of Electrical and Computer Engineering, Director, Micro and Nanotechnology Laboratory, University of Illinois at Urbana – Champaign, Urbana, IL 61801, USA.
#Authors contributed equally

advanced biosensing structure consists of a graphene sheet (the sensing element) embedded in between two dielectric layers which insulate the graphene from electrochemical basal plane reactions in electrolyte solution[17]. High-k dielectric materials are being widely adopted by the semiconductor industry for the fabrication of state-of-the-art CMOS transistors due to their superior gate oxide capacitance values when compared to traditional materials such as $SiO_2$. Robust, high-k oxides that are capable of being incorporated in aqueous environments are of interest for biosensing applications where a large gate capacitance is required. In particular, hafnium oxide ($HfO_2$) has attracted widespread interest by the biosensor community due to its chemical stability, pH sensitivity, and a high-k dielectric constant which has reported values of 20–25[19–21]. $HfO_2$ also has an isoelectric point of 7.0[22], making its surface neutral at physiological pH. Thus, $HfO_2$ is both a suitable alternative for nanopore membrane materials and ideal for integration with stacked graphene-dielectric biosensors. While the material properties of $HfO_2$ are well studied and applicable in the semiconductor industry, to our knowledge, there have not been any studies done on $HfO_2$ as a candidate material for nanopore bio-sensing applications. In this work, we investigate the electrical properties and hydrophilicity of as-deposited and annealed $HfO_2$ films in solution to explore the viability of $HfO_2$ as both a new nanopore sensor material and a potential high-k nanopore transistor material. We also analyzed noise characteristics in the nanopore for annealed and as-deposited membranes to verify pore wettability. Finally, we show DNA translocation through $HfO_2$ nanopores.

## RESULTS AND DISCUSSION

The schematic diagram in Figure 1a shows the fabrication process for the $HfO_2$ membrane. A supporting 80μm wide membrane consisting of stacked $Al_2O_3$/ $SiN_x$ /$Al_2O_3$ layers was suspended on a 300 μm-thick Si wafer using a Bosch etching process (See Methods section for more details). The bottom $Al_2O_3$ layer acts as an etch stop layer for the opening of 80 μm wide backside trench by DRIE. The low stress $SiN_x$ layer is deposited for reduced noise and increased robustness. The top $Al_2O_3$ layer is added as a hydrophilic layer on top of the $SiN_x$ for improved graphene transfer process[17]. A 300 nm hole was formed in the supporting membrane using a focused ion beam. The circular shaped pore was covered by a graphene layer, on which an $HfO_2$ membrane was grown using atomic layer deposition.

Intrinsic stresses and pinholes present in nanolaminates are deleterious to ultra-thin membrane fabrication, a necessary step to achieving highly sensitive nanopore sensors. The high breaking and intrinsic strength of graphene[23] make the material well suited for instances where a free-standing membrane is required, as demonstrated by the recent fabrication of oxide membranes on graphene[24]. Graphene is a single layered hexagonal sheet of $sp^2$ hybridized carbon atoms with remarkable mechanical characteristics and electrical properties[25]. Graphene is used here for mechanical support for our $HfO_2$ structures but easy to drill through using the electron beam. In addition, the graphene-dielectric stack methodology leaves room for the incorporation of a gate bias in future applications where conductance modulation is required. $HfO_2$ was deposited using atomic layer deposition (ALD) on a graphene surface. ALD was chosen since it allows for conformal, low temperature, and sub-nanometer deposition control. The lack of dangling bonds on the basal plane of graphene makes atomic layer deposition difficult since there are no available sites for nucleation[26]. For this reason, a thin metal seed layer was evaporated on graphene. Titanium was chosen as the seed layer due to its high adsorption energy on graphene[27] and low surface diffusion[28]. The 2 nm film of titanium was oxidized once exposed to air, resulting in a thin layer of $TiO_2$ on the graphene surface.

The composite membrane was then imaged using transmission electron microscopy (TEM). Figure 1b and 1c show TEM images and corresponding FFT images, respectively. The as-deposited $HfO_2$ membrane on the functionalized graphene surface is shown in Figure 1b(i~iii). Figure 1b(i) shows the $HfO_2$ membrane before drilling a nanopore, where the amorphous phase of the as-deposited membrane was observed using TEM and confirmed by taking a Fast Fourier Transform (FFT) depicted in Figure 1b(i'). Figure 1b(ii) and 1c(ii′) depict changes in membrane structure after being exposed to a focused electron beam for drilling a nanopore. Crystallization of the as-deposited film was observed in the vicinity of the nanopore in as-deposited membrane after pore formation. This was a very interesting finding because as-deposited $HfO_2$ films prepared by atomic layer deposition are typically amorphous and known to crystallize in the monoclinic phase at relatively low temperatures (~500 °C)[29, 30]. To verify if the crystallization was formed by nanopore drilling process, another region on the same membrane, ~ 70 nm away from nanopore region, was examined and it remained in the as-deposited amorphous phase as shown in Figure 1b(iii) and confirmed by 1c(iii′). As a control, nanopores were drilled in membranes annealed at 500 °C. The crystallized membranes are shown in Figure 1b (iv~vi) and 1c(iv′~vi′). Annealed membranes exhibited a crystalline pattern before exposed to the focused electron beam as shown in Figure 1b (iv). The corresponding FFT images confirm the crystalline structure of annealed $HfO_2$ membranes as shown in Figure 1c (iv′~vi′). We further investigated with $SiN_x$ membrane (Protochips, NC), and as expected, found no crystallization in the membrane after drilling a nanopore (see Supplementary Information Figure S1). Previously, a study on $Al_2O_3$ reported hexagonal nanocrystallites in the vicinity of a nanopore in $Al_2O_3$ membrane, while SiN membrane found no crystallinity after pore formation[31]. However, crystallization in the vicinity of the nanopore is a unique characteristic of as-deposited $HfO_2$ membranes after being exposed to a focused electron beam for pore formation. We demonstrated the electron beam induced local-crystallization in the vicinity of the nanopore area in $HfO_2$ membranes on graphene, and it is postulated that the local-crystallization is a result of heating from the electron beam irradiation[32, 33]. In the past, reports have shown that heat treatment of $HfO_2$ films results in improved electrical characteristics due to reduced oxygen vacancies, passivation of interface traps, and overall improvement in dielectric constant[34]. However, there is also the possibility of introducing oxygen depleted states through grain boundary formation during the heating phase[35]. Increased hydrophilicity of insulators, an essential material property for nanopore sensors due to the spontaneous evaporation of water in confined nanoscale spaces[36], has also been attributed to high temperature annealing.

To study the effects of crystallization on the electrical properties of $HfO_2$, we annealed $HfO_2$ films deposited by atomic layer deposition in $Ar/H_2$ gas for 20 minutes at 500 °C and 700 °C. As-deposited and annealed $HfO_2$ films were characterized in an electrolyte-oxide-silicon configuration to ascertain dielectric quality in nanopore experiment condition (typically 1M KCl, pH 7.4). 16 nm thick $HfO_2$ films were deposited on polished, highly doped p-type silicon (p<5 mOhm-cm) using atomic layer deposition. The electrolyte solution (1M KCl at pH 7.4 containing 10 mM Tris and 1 mM EDTA) was dispensed onto a 2.5 mm diameter PDMS well on the $HfO_2$ surface and connected using Ag/AgCl electrodes while the back of the silicon substrate was connected to ground. As shown in Figure 2a, we first applied voltages in the range between −500 mV and +500 mV across the electrolyte-dielectric interface using Axopatch 200B (Molecular Devices, CA) and acquired the data traces through Digidata 1440A (Molecular Devices, CA). The leakage current density in this voltage range is approximately 6.6 $pA/mm^2$ and 13 $pA/mm^2$ for both as-deposited and 500 °C annealed (crystallized) films, but the 700 °C annealed film showed 2.8 $nA/mm^2$ of leakage current at 500 mV. We further investigated the leakage current as a function of voltage using a Keithley 237 controlled by LabView software. The leakage current behavior changes drastically at 3V where an exponential increase is observed for as-deposited $HfO_2$ and $HfO_2$ annealed at both 500 °C and at 700 °C. Annealed $HfO_2$ films showed intolerable leakage current. The leakage density of 500 °C crystallized $HfO_2$ is ~$10^{-9}$ $A/mm^2$ and 700

°C crystallized $HfO_2$ for ~$10^{-8}$ A/mm$^2$ at 2V, while the as-deposited film is $10^{-11}$ A/mm$^2$. The increase in leakage currents at a lower voltage for annealed films is attributed to microstructural changes during the growth of grain boundaries in the dielectric after post-deposition annealing. Previous studies report similar breakdown behavior for amorphous $HfO_2$ films on p-type silicon in aqueous environment[37], however our results are the first extracted in a fluidic (1M KCl at pH 7.4) environment for crystallized films. To further investigate the feasibility of integrating a gate bias with our architecture for ionic field effect regulation in the nanopore, we measured leakage current density through the $HfO_2$ deposited on graphene (see Supplementary Information Figure S2).

In addition to analyzing electrical characteristics, we studied the effects of crystallization on the wettability of $HfO_2$ films. Theoretical studies predict that liquids confined in between hydrophobic surfaces with contact angles approaching 90° are prone to spontaneous evaporation[38]. The hydrophobicity of nanopores can be beneficial in voltage and pressure induced gating applications, however it can present a hindrance to DNA translocation nanopore experiments due to wetting difficulties. The hydrophilicity of the surface was analyzed for $HfO_2$ deposited on both metal-seeded graphene and p-type silicon in order to assess the impact of crystallization on nanopore functionality. The equilibrium contact angle was determined using a profile fitting method based on Young's equation. Contact angle values were measured using an Attension goniometer (Biolin Scientific, Finland). As expected, 16 nm ALD $HfO_2$ deposited on the graphene and silicon surfaces showed almost identical contact angle as confirmed in Figure 2c. Interestingly, there was an increase in hydrophilicity for both surfaces after post-deposition annealing. The influence of post-deposition annealing on the contact angle of dielectric films is known as thermo-induced hydrophilicity[39, 40]. This effect is attributed to the removal of surface contaminants, crystal phase transition, and changes in porosity during annealing[39]. Figure 2c shows a contact angle difference of approximately 10° degrees for as-deposited $HfO_2$ in comparison with films that have been annealed at 500 °C. The contact angle for $HfO_2$ on p-silicon and graphene decreased to 39° and 30° respectively after annealing at 700 °C. Notably, we found that traditionally used $Si_3N_4$ films are much more hydrophobic with contact angles of 75 ° (see Supplementary Information Figure S3). Similar to earlier reports on thermo-induced hydrophilicity, increasing annealing temperature results in superior hydrophilicity of the oxide film. Hence, increased hydrophilicity and improved wettability is expected in the pore region due to localized heating and subsequent crystallization resulting from electron beam irradiation[41].

In solid state nanopores, 1/f noise has been attributed to a variety of physical factors including surface charge fluctuations[42] as well as the mobility of charge carriers[43] at the nanopore surface. Excessive 1/f noise has also been attributed to nanobubbles present in the nanopore[43] and has been shown to be reduced by addition of a hydrophilic oxide layer[44]. In addition, oxygen plasma and chemical treatments are known to reduce 1/f noise and make the pore more hydrophilic. Figure 3(a) shows a 1/f noise values comparison of nanopores between as-deposited and annealed $HfO_2$ membrane at 500 °C from 100 to 300 mV. Nanopores in similar size were used for 1/f noise measurement, 2 × 3 nm pore in as-deposited and 2.2 × 2.8 nm pore for annealed $HfO_2$ membrane. Interestingly, nanopores in both of as-deposited and annealed $HfO_2$ produced very similar 1/f noise value. Similar 1/f noise between as-deposited and annealed membrane confirm that the 1/f noise is dominated by local charge interactions in the nanopore region as opposed to being affected by the bulk phase transition. This was confirmed by imaging the local-crystallization at the nanopore region on amorphous as-deposited and crystallized $HfO_2$ membranes (Figure 1b and 1c). In addition, Figure 3b shows current versus voltage measurements for five different $HfO_2$ nanopore diameters. These measurements were taken by mounting the nanopore chip in between two reservoirs that were later filled with conductive electrolyte (1M KCl at pH 7.4).

Figure 3b shows that the relationship between current and voltage for a nanopore submerged in conductive solution approximates Ohm's law. The I/V measurements through multiple nanopores were in good agreement with previous findings for open pore current[45] without any asymmetric or rectifying currents.

Furthermore, we detected dsDNA translocation with our $HfO_2$ nanopore sensor. The experiment was performed in 1 M KCl, 10 mM Tris, 1 mM EDTA, pH 7.2 and the concentration of DNA was 1 nM. In this experiment, 1 kbp dsDNA was introduced to the *cis* side of the chamber followed by an applied bias of 500 mV at the *trans* side. Applying negative voltages to the *trans* side or replacing the dsDNA with blank 1M KCl solution resulted in no current blockages, indicating that the observed events are from DNA translocation. The magnitude of the translocation event will depend on the pore geometry and size of the translocating molecule.

Assuming a cylindrical geometry, the ionic current through a circular nanopore is defined by $=\frac{\sigma AV}{l}$, where σ is the conductivity of the electrolyte solution, A is the cross-sectional area of the nanopore, V is the applied bias, and l is the length of the pore. Consequently, the percent change in open pore current follows the relationship $\Delta I / I = \Delta A / A$ where ΔA and A are the cross-sectional area of the molecule and nanopore, respectively[46]. Hundreds of events were detected with numbers in proportion to the applied voltage level; 172 events at 200 mV, 92 at 300 mV, 118 at 400 mV and 351 at 500 mV. Figure 4a shows representative ionic current traces of 1 kbp dsDNA through a 4 nm pore in $HfO_2$ membrane. Nanopore ionic signature shows decrease in magnitude with decreasing voltage, indicating that DNA molecules are directly changing the ionic conductance of the nanopore. Figure 4b shows a set of current blockade values resulting from applied voltages in the range of 200–500 mV. Current blockades were obtained fitting a Gaussian function to peak blocking current, and showed nanopore ionic current blocking of 285.5 pA at 200 mV, 384.9 pA at 300 mV, 515.3 pA at 400 mV and 623.8 pA at 500 mV, which are in good agreement with the standard geometric model (see Supplementary Information Figure S4). In addition, there is a translocation dwell time associated with each applied voltage. Ionic current signature shows shortened translocation duration with increasing voltage, indicating that translocations of DNA molecules are voltage-driven. Figure 4c shows a set of translocation duration values obtained by Exponential fittings to translocation dwell time in applied voltages from 200 mV to 500 mV. The obtained duration values were 318 μs at 200 mV, 115 μs at 300 mV, 88 μs at 400 mV and 58 μs at 500 mV (see Supplementary Information Figure S4). The trend of decrease in translocation duration with increasing voltage can be well fitted to an exponential function, which is found in previous report and expected in translocation of DNA through solid-state nanopores[47].

## CONCLUSIONS

The aim of this work was to demonstrate DNA detection using $HfO_2$ based nanopore sensors. Graphene, a single layered hexagonal sheet of $sp^2$ carbon atoms grown by chemical vapor deposition, was used as a structural support in the fabrication of $HfO_2$ membranes. Transmission electron microscopy was used to drill a single nanometer sized hole in the membrane. Locally induced crystallization of $HfO_2$ was observed upon prolonged exposure of the electron beam during nanopore drilling, a consequence that is attributed to localized heating. In order to elucidate the effects of crystallization on the electrical and surface properties of $HfO_2$, ultra-thin films were deposited via atomic layer deposition on p-type silicon and characterized in 1M KCl solution. Leakage currents were analyzed for annealed and as-deposited films, revealing higher current densities in crystallized films due to the nucleation of grain boundaries.

However, crystallization of the high k dielectric resulted in increased hydrophilicity, suggesting improved wettability in $HfO_2$ nanopores. Power spectral density plots were acquired and the 1/f noise was shown to scale under increasing applied voltages for both as-deposited and annealed films, suggesting good pore wettability. Finally, the viability of $HfO_2$ nanopores as a biosensing platform was verified by performing DNA translocation experiments. We conclude that $HfO_2$ is a suitable material for nanopore sensing applications due to its potential in high-k nanopore transistor applications, thermo-induced hydrophilicity, chemical inertness, and the ability to detect DNA transport.

## Methods

### Supporting membrane fabrication

Supporting membrane fabrication process has been introduced in previous study[17], and brief description is as follow. Membranes were fabricated on 300 ± 2 µm thick double-side polished <100> silicon wafers (Quest International). Wafers were cleaned in piranha solution (1:2 ratios of $H_2SO_4$ and $H_2O_2$) for 15 minutes, DI-water rinsed and air-gun dried before depositing $Al_2O_3$ via Atomic Layer Deposition (ALD Cambridge Nanotech). 50 nm of $Al_2O_3$ was deposited at a platen temperature of 250 °C using tetramethyl-aluminum (TMA) and water vapor precursors. Subsequently, 200 nm of low-stress $SiN_x$ was deposited (STS Mesc PECVD system) using a mixed-frequency recipe (high frequency, 6 sec at 13.56 Mhz, platen power of 20W; and low frequency, 2 sec at 380 kHz, platen power of 60 W) with precursors silane ($SiH_4$) and ammonia ($NH_3$) at flow rates of 40 and 55 sccm, respectively, at a platen temperature of 300 °C. Another 50 nm of $Al_2O_3$ is deposited via ALD on the $SiN_x$ layer as described above, resulting in stacked $Al_2O_3$/ $SiN_x$ / $Al_2O_3$ layers. The backside of the wafer is then spin-coated with Megaposit SPR220 photoresist (3000 rpm at 30 sec followed by soft bake at 60 °C for 2 min and 110 °C for 1 min). Optical lithography is used to pattern 80µm square windows on the backside of the water while the front side is protected with KMPR 1000 photoresist. The wafer is later placed into an STS Pegasus ICP DRIE and back-etched for 22 minutes using a Bosch etching process. This process results in the suspension of 80µm wide square membrane of stacked layers (the bottom $Al_2O_3$layer serves as a stop layer). Finally, a focused ion beam (FEI FIB DB235) operated at a beam current of 30 pA is used to form 300 nm hole on the suspended stacked membrane.

### Graphene and $HfO_2$ nanopore fabrication

Graphene was grown via chemical vapor deposition (CVD) on 1.4 mil copper foil (Alfa Aesar). The copper foil was placed in an Atomate CVD furnace and annealed at 1000 °C under Ar/H2 flow for 90 minutes at a base pressure of ~4.4 torr in order to increase the copper grain size. Graphene is grown for 50 minutes at 1000 °C under 125 sccm of CH4 and 50 sccm of $H_2$ at a base pressure of about 2.5 Torr. Once the graphene is grown on the copper, the substrate is cooled to room temperature under 500 sccm of Ar while the base pressure is ramped up to 760 Torr. The copper foil is then coated with two layers of PMMA (295 K A2 and 950 K A4). Both layers are spun at 3000 rpm for 30 seconds and soft-baked for 2 minutes at 200C. The graphene grown on the backside of the copper foil is then etched away by an O2 plasma etching process (Plasmatherm Freon RIE). After graphene removal from the backside, the copper is etched away overnight in $FeCl_3$ solution (Transcene CE-100). The resulting graphene film protected by the PMMA bilayer is then transferred from the copper etchant to DI water using a piranha-cleaned (1:2 ratio of $H_2SO_4$:$H_2O_2$) glass slide.

Subsequently, the film is transferred to 10% hydrochloride (HCl) solution diluted in DI water to remove residual metal particles followed by a second DI water rinse. The film is then transferred onto a 12 × 12 mm chip with our predefined FIB holes (about 300 nm in diameter) and the PMMA is removed by submerging the chip in 1:1 methylene chloride/methanol solution for 30 minutes. The samples are subsequently annealed in an Ar(500 sccm)/$H_2$(100 sccm) environment for 1.5 hours to remove PMMA residue from the surface. Samples were then placed inside of a CHA SEC-600 electron beam evaporator after the graphene transfer and anneal was completed. An ultra-thin, 2 nm seed layer of titanium oxide ($TiO_2$) was evaporated over the graphene substrate at a rate of 0.2A/sec. The graphene/$TiO_2$ chips were then placed inside an ALD reactor and 16 nm of $HfO_2$ was deposited over the surface at a platen temperature of 200 °C. Single nanopores ranging from 1 to 5 nm in diameter were drilled using a transmission electron microscope (JEOL 2010F field-emission gun) operated at 200 kV in convergent beam electron diffraction (CBED) mode with a focused electron probe of diameter ~ 1.5 nm. An O2 plasma treatment on the backside of the chip was performed at 50W for 30 sec to remove hydrophobic graphene layer and to facilitate nanopore wetting.

## Supplementary Material

Refer to Web version on PubMed Central for supplementary material.

## Acknowledgments

The authors would like to acknowledge funding support from Oxford Nanopore Technologies, U.K and the National Institutes of Health (Grant # R21 CA155863). The authors would also like to acknowledge valuable discussions with Shouvik Banerjee and David Estrada. In addition, the support from the staff of the Micro and Nanotechnology Laboratory (MNTL) is greatly appreciated.

## References

1. Venkatesan BM, Bashir R. Nanopore sensors for nucleic acid analysis. Nat Nanotechnol. 2011; 6:615–624. [PubMed: 21926981]
2. Branton D, et al. The potential and challenges of nanopore sequencing. Nat Biotechnol. 2008; 26:1146–1153. [PubMed: 18846088]
3. Wanunu M. Nanopores: A journey towards DNA sequencing. Phys Life Rev. 2012; 9:125–158. [PubMed: 22658507]
4. Gu LQ, Shim JW. Single molecule sensing by nanopores and nanopore devices. Analyst. 2010; 135:441–451. [PubMed: 20174694]
5. Howorka S, Siwy Z. Nanopore analytics: sensing of single molecules. Chem Soc Rev. 2009; 38:2360–2384. [PubMed: 19623355]
6. Wanunu M, et al. Nanopore Analysis of Individual RNA/Antibiotic Complexes. Acs Nano. 2011; 5:9345–9353. [PubMed: 22067050]
7. Smeets RMM, Kowalczyk SW, Hall AR, Dekker NH, Dekker C. Translocation of RecA-Coated Double-Stranded DNA through Solid-State Nanopores. Nano Lett. 2009; 9:3089–3095. [PubMed: 19053490]
8. Shim J, et al. Detection and Quantification of Methylation in DNA using Solid-State Nanopores. Sci Rep-Uk. 2013; 3
9. Singer A, Rapireddy S, Ly DH, Meller A. Electronic Barcoding of a Viral Gene at the Single-Molecule Level. Nano Lett. 2012; 12:1722–1728. [PubMed: 22352964]
10. Venta K, et al. Differentiation of Short, Single-Stranded DNA Homopolymers in Solid-State Nanopores. Acs Nano. 2013
11. Paik KH, et al. Control of DNA Capture by Nanofluidic Transistors. Acs Nano. 2012; 6:6767–6775. [PubMed: 22762282]
12. Jiang ZJ, Stein D. Charge regulation in nanopore ionic field-effect transistors. Phys Rev E. 2011; 83

NIH-PA Author Manuscript
NIH-PA Author Manuscript




13. Nam SW, Rooks MJ, Kim KB, Rossnagel SM. Ionic Field Effect Transistors with Sub-10 nm Multiple Nanopores. Nano Lett. 2009; 9:2044–2048. [PubMed: 19397298]
14. Xie P, Xiong QH, Fang Y, Qing Q, Lieber CM. Local electrical potential detection of DNA by nanowire-nanopore sensors. Nat Nanotechnol. 2012; 7:119–125. [PubMed: 22157724]
15. Schneider GF, et al. DNA Translocation through Graphene Nanopores. Nano Lett. 2010; 10:3163–3167. [PubMed: 20608744]
16. Merchant CA, et al. DNA Translocation through Graphene Nanopores. Nano Lett. 2010; 10:2915–2921. [PubMed: 20698604]
17. Banerjee S, et al. Electrochemistry at the Edge of a Single Graphene Layer in a Nanopore. Acs Nano. 2013; 7:834–843. [PubMed: 23249127]
18. Venkatesan BM, et al. Stacked Graphene-Al2O3 Nanopore Sensors for Sensitive Detection of DNA and DNA-Protein Complexes. Acs Nano. 2012; 6:441–450. [PubMed: 22165962]
19. Dorvel BR, et al. Silicon Nanowires with High-k Hafnium Oxide Dielectrics for Sensitive Detection of Small Nucleic Acid Oligomers. Acs Nano. 2012; 6:6150–6164. [PubMed: 22695179]
20. Wilk GD, Wallace RM, Anthony JM. High-kappa gate dielectrics: Current status and materials properties considerations. J Appl Phys. 2001; 89:5243–5275.
21. Robertson J. High dielectric constant oxides. Eur Phys J-Appl Phys. 2004; 28:265–291.
22. Parks GA. Isoelectric Points of Solid Oxides Solid Hydroxides and Aqueous Hydroxo Complex Systems. Chem Rev. 1965; 65:177–&.
23. Lee C, Wei XD, Kysar JW, Hone J. Measurement of the elastic properties and intrinsic strength of monolayer graphene. Science. 2008; 321:385–388. [PubMed: 18635798]
24. Wang LD, et al. Ultrathin Oxide Films by Atomic Layer Deposition on Graphene. Nano Lett. 2012; 12:3706–3710. [PubMed: 22716769]
25. Zhang YB, Tan YW, Stormer HL, Kim P. Experimental observation of the quantum Hall effect and Berry's phase in graphene. Nature. 2005; 438:201–204. [PubMed: 16281031]
26. Fallahazad B, et al. Scaling of Al2O3 dielectric for graphene field-effect transistors. Appl Phys Lett. 2012; 100
27. Chan KT, Neaton JB, Cohen ML. First-principles study of metal adatom adsorption on graphene. Phys Rev B. 2008; 77
28. Matsubayashi A, Abel J, Sinha DP, Lee JU, LaBella VP. Characterization of metal oxide layers grown on CVD graphene. J Vac Sci Technol A. 2013; 31
29. Kim H, McIntyre PC, Saraswat KC. Effects of crystallization on the electrical properties of ultrathin HfO2 dielectrics grown by atomic layer deposition. Appl Phys Lett. 2003; 82:106–108.
30. Kim H, Marshall A, McIntyre PC, Saraswat KC. Crystallization kinetics and microstructure-dependent leakage current behavior of ultrathin HfO2 dielectrics: In situ annealing studies. Appl Phys Lett. 2004; 84:2064–2066.
31. Venkatesan BM, et al. Highly Sensitive, Mechanically Stable Nanopore Sensors for DNA Analysis. Adv Mater. 2009; 21:2771–+. [PubMed: 20098720]
32. Liu LC, Risbud SH. Real-Time Hot-Stage High-Voltage Transmission Electron-Microscopy Precipitation of Cds Nanocrystals in Glasses - Experiment and Theoretical-Analysis. J Appl Phys. 1994; 76:4576–4580.
33. Yokota T, Murayama M, Howe JM. In situ transmission-electron-microscopy investigation of melting in submicron Al-Si alloy particles under electron-beam irradiation. Phys Rev Lett. 2003; 91
34. Yang WL, Marino J, Monson A, Wolden CA. An investigation of annealing on the dielectric performance of TiO2 thin films. Semicond Sci Tech. 2006; 21:1573–1579.
35. Baik HS, et al. Interface structure and non-stoichiometry in HfO2 dielectrics. Appl Phys Lett. 2004; 85:672–674.
36. Smirnov S, Vlassiouk I, Takmakov P, Rios F. Water Confinement in Hydrophobic Nanopores. Pressure-Induced Wetting and Drying. Acs Nano. 2010; 4:5069–5075. [PubMed: 20690599]
37. Wallrapp F, Fromherz P. TiO2 and HfO2 in electrolyte-oxide-silicon configuration for applications in bioelectronics. J Appl Phys. 2006; 99

38. Luzar A. Activation barrier scaling for the spontaneous evaporation of confined water. J Phys Chem B. 2004; 108:19859–19866.
39. Ye Q, Liu PY, Tang ZF, Zhai L. Hydrophilic properties of nano-TiO2 thin films deposited by RF magnetron sputtering. Vacuum. 2007; 81:627–631.
40. Azimirad R, Naseri N, Akhavan O, Moshfegh AZ. Hydrophilicity variation of WO3 thin films with annealing temperature. J Phys D Appl Phys. 2007; 40:1134–1137.
41. Kim HM, Lee MH, Kim KB. Theoretical and experimental study of nanopore drilling by a focused electron beam in transmission electron microscopy. Nanotechnology. 2011; 22
42. Stein D, Kruithof M, Dekker C. Surface-charge-governed ion transport in nanofluidic channels. Phys Rev Lett. 2004; 93
43. Smeets RMM, Keyser UF, Wu MY, Dekker NH, Dekker C. Nanobubbles in solid-state nanopores. Phys Rev Lett. 2006; 97
44. Chen P, et al. Atomic layer deposition to fine-tune the surface properties and diameters of fabricated nanopores. Nano Lett. 2004; 4:1333–1337.
45. Smeets RMM, et al. Salt dependence of ion transport and DNA translocation through solid-state nanopores. Nano Lett. 2006; 6:89–95. [PubMed: 16402793]
46. Storm AJ, Chen JH, Zandbergen HW, Dekker C. Translocation of double-strand DNA through a silicon oxide nanopore. Phys Rev E. 2005; 71
47. Wanunu M, Sutin J, McNally B, Chow A, Meller A. DNA Translocation Governed by Interactions with Solid-State Nanopores. Biophys J. 2008; 95:4716–4725. [PubMed: 18708467]

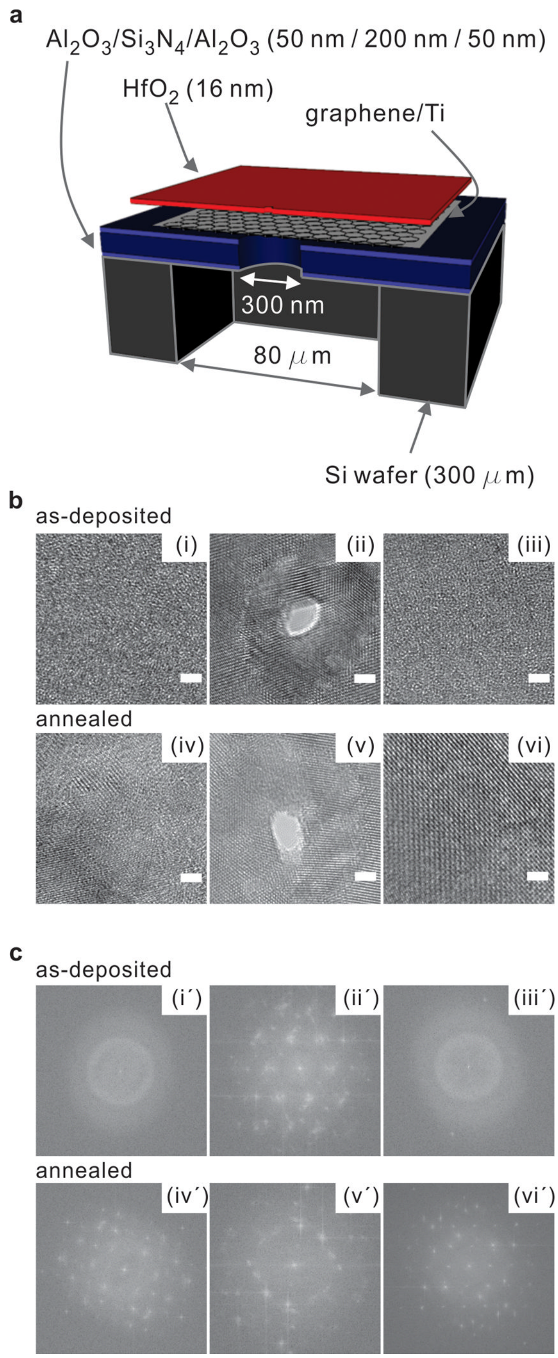


**Figure 1. Schematic of membrane fabrication and TEM images with its corresponding FFT images**

a) Schematic cross-section of our membrane architecture. b) TEM phase contrast images of as-deposited amorphous (i~iii) and annealed (iv~vi) $HfO_2$ films deposited on a graphene supported membrane. (i) As-deposited $HfO_2$ membrane before being exposed to a focused electron beam for drilling a nanopore. (ii) A nanopore drilled in amorphous $HfO_2$ film showing electron beam induced crystallinity in the vicinity of the pore. (iii) $HfO_2$ bulk phase which is ~70 nm away from a focused electron beam remains amorphous after a nanopore formation. (iv) Annealed $HfO_2$ membrane before being exposed to a focused electron beam. (v) A nanopore was drilled in annealed $HfO_2$ membrane. (vi) Annealed $HfO_2$ bulk phase which is ~70 nm away from a focused electron beam. (iv~vi) Annealed $HfO_2$ membrane showed crystallinity at all stages. c) FFTs of corresponding TEM image found in Figure 1a confirming amorphous (i', iii') and crystallized (ii', iv', v', vi') phases before and after nanopore formation.

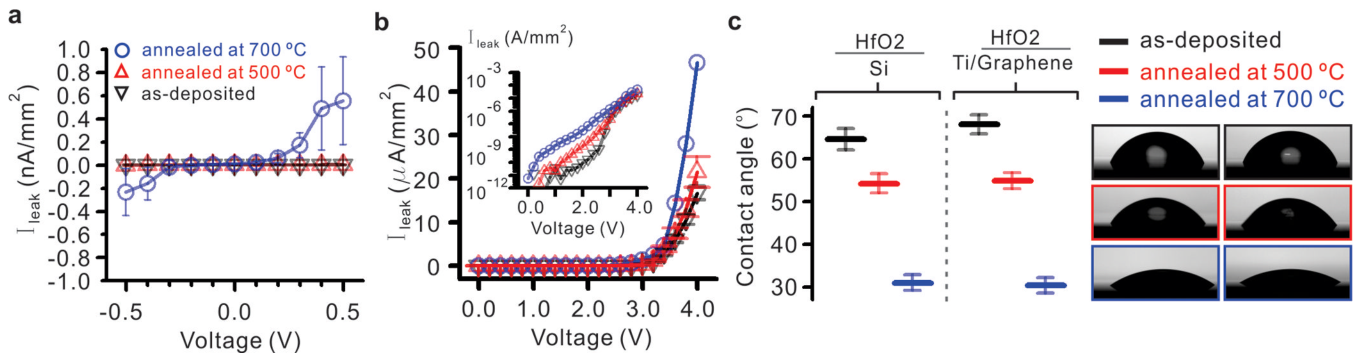


**Figure 2. Characterization of ALD $HfO_2$ film in an aqueous environment**

(a) Leakage current densities for as-deposited and annealed $HfO_2$ films in an electrolyte-oxide-silicon configuration. (b) The dielectric breakdown of $HfO_2$ for higher voltages in 1M KCl, where the annealed films show a higher leakage characteristic. (c) The contact angle for $HfO_2$ on silicon and for $HfO_2$ on metal-seeded graphene decreases after annealing at 500 °C and 700 °C, indicating thermo-induced hydrophilicity due to a crystal phase transition.

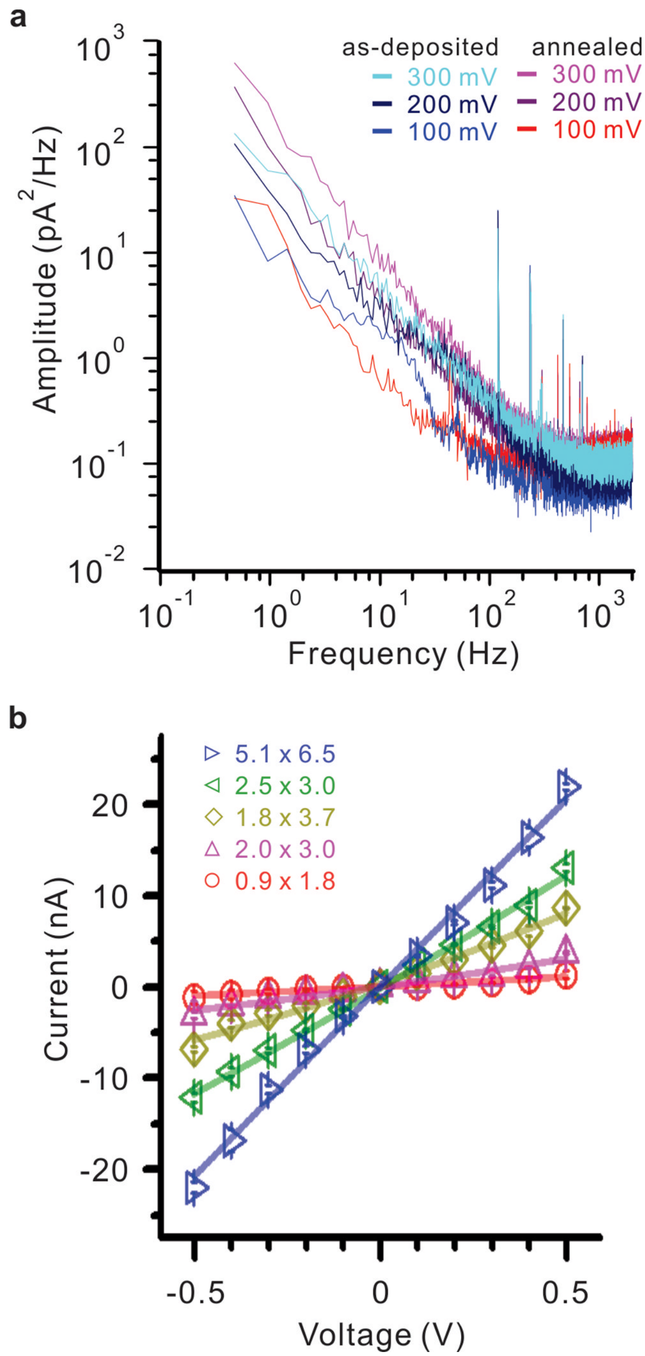


**Figure 3. Noise and I-V characteristics for nanopores drilled in $HfO_2$**

(a) The magnitude of the 1/f noise scales with the applied voltage, indicating wettability of the pore. In comparison between annealed values and as-deposited values of 1/f noise are similar in magnitude, suggesting that the 1/f noise is dominated by ionic interactions at the crystallized nanopore as opposed to being influenced by the phase of the bulk membrane region. The nanopores used for 1/f noise measurement are in similar dimension. As-deposited membrane has 2 × 3 nm pore and annealed membrane has 2.2 × 2.8 nm. (b) IV curve measurement for five nanopores of different sizes in 1M KCl solution.

NIH-PA Author Manuscript
NIH-PA Author Manuscript



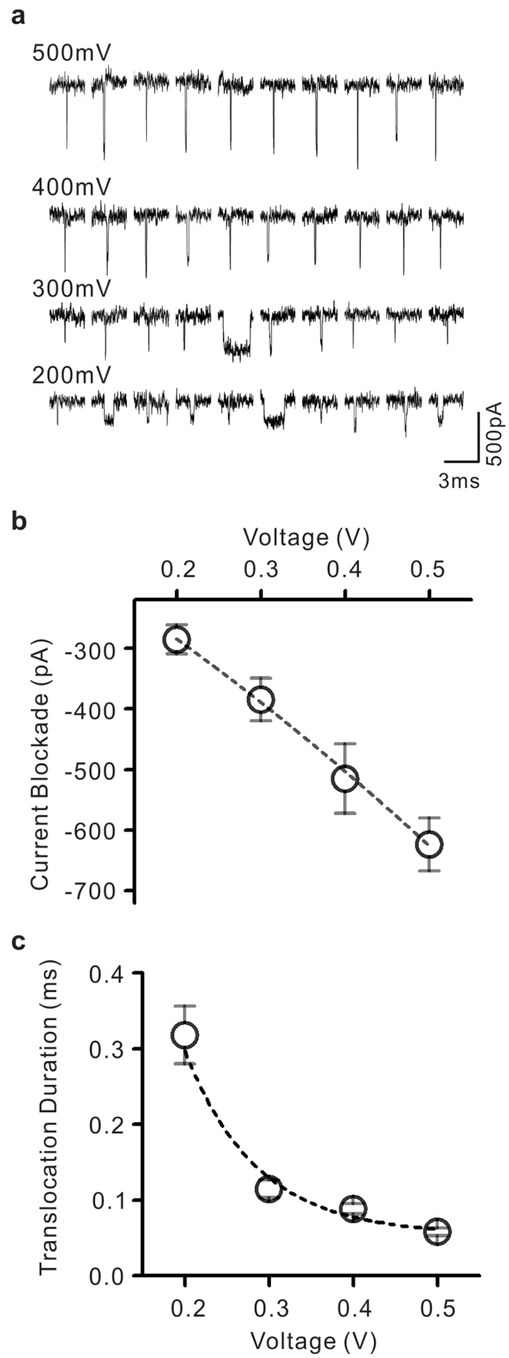


**Figure 4. Double-stranded DNA translocation**

(a) Representative data traces showing translocation of 1 kbp dsDNA through a 4 nm pore in $HfO_2$ membrane. Nanopore ionic currents were recorded in 1M KCl at pH 7.4 containing 10 mM Tris and 1 mM EDTA at voltages in range from 200 mV to 500 mV. (b) Current blockade levels for DNA translocation events plotted as a function of voltage. (c) Translocation durations of the events corresponding to four different voltages. The values of current blockades and translocation durations were obtained by fitting to a Gaussian function and an Exponential function, respectively